Composite Structures 160 (2017) 653–669

Contents lists available at ScienceDirect

Composite Structures

journal homepage: www.elsevier.com/locate/compstruct

Elastostatic analysis of two-directional functionally graded beams using various beam theories and Symmetric Smoothed Particle Hydrodynamics method

Armağan Karamanlı

Department of Mechatronics, Faculty of Engineering and Architecture, Istanbul Gelişim University, 34215 Istanbul, Turkey

ARTICLE INFO

Article history:
Received 1 August 2016
Available online 27 October 2016

Keywords:
Meshless method
Functionally graded beam
Bending deflection
SSPH method
Shear deformation theories

ABSTRACT

The elastostatic behaviour of two-directional functionally graded beams (FGBs) subjected to various sets of boundary conditions are investigated for the first time by using the Euler-Bernoulli, Timoshenko and Reddy-Bickford beam theories and the Symmetric Smoothed Particle Hydrodynamics (SSPH) method. To validate the developed code, a simply supported conventional FGB problem is studied and the comparison studies are performed along with the analytical solutions and the results from previous studies. The numerical calculations in terms of maximum dimensionless transverse deflections, dimensionless axial and transverse shear stresses are performed based on different beam theories with varying gradation exponents (power-law index), different aspect ratios (L/h) and sets of boundary conditions.

1. Introduction

One of the biggest problems that the engineers face with during the new product development process is the selecting of the proper material to be used for the engineering applications. There are many factors to be considered for the optimization of the selection process such as the cost of raw material and production, fabrication techniques, logistics, material properties, requirements of customers with severe operating conditions. For instance; the material should be hard but also ductile or the material can withstand very high surface temperature of 2000 K and a temperature gradient of 1000 K across a 10 mm thickness and so on. In 1984, a group of Japanese scientists working on a space shuttle project requiring a thermal barrier with high performance properties introduced a novel material called Functionally Graded Material (FGM). FGMs can be classified as advanced materials which are inhomogeneous and made up of two (or more) different materials combined in solid states with varying properties as the dimension changes.

Among many modern engineering applications of the FGMs, the most important ones are the aerospace, biomedical, defence, energy, optoelectronics, automotive (engine components), turbine blade, reactor components (nuclear energy) and etc. FGMs may be used in different application areas with the development of new fabrication technologies, the reduction in cost of production, improvement in the properties of FGMs.

The advantages of the FGMs over the conventional and classical composite materials are basically due to varying material properties over a changing dimension which allow to enhance the bond strength through the layer interfaces, high resistance to temperature shocks, lower transverse shear stresses, etc. Researchers have been devoted a considerable number of studies to predict and to understand the mechanics of the FGM structures during the last decade [1–31].

It is seen from the above literature survey that the most of the analyses are related to conventional FGMs (or 1D-FGM) with material properties which vary in one direction. However, there are practical engineering applications as stated in [32], the conventional FGMs are not efficient to fullfill the technical requirements such as the temperature and stress distributions in two or three directions for aerospace craft and shuttles.

To eliminate mentioned drawback of the conventional FGM, a new type FGM whose material properties can vary in two or three directions is needed. Motivated by this fact, the mechanical and thermal behaviours of two-directional FG structures have been investigated so far. For instance, by using the Element Free Galerkin Method, 2D steady-state free and forced vibrations of two-directional FGBs are analysed in [33]. The elasticity solutions are proposed for bending and thermal deformations of FGBs with various end conditions by using the state-space based differential quadrature method in [34]. A semi-inverse method was employed to investigate buckling of axially functionally graded beam [35]. The buckling of non-uniform axially graded beams was studied with varying flexural rigidity based on the EBT in [36]. A

E-mail address: armagan_k@yahoo.com

http://dx.doi.org/10.1016/j.compstruct.2016.10.065
0263-8223/

symplectic elasticity solution for static and free vibration analyses of two-directional FGBs with the material properties varying exponentially in both axial and thickness direction is presented in [37]. The buckling of Timoshenko beams composed of two dimensional FGM was studied in [38].

As it is seen form above discussions, the studies related to analytical and semi-analytical solutions of two-directional FGBs which have complex governing equations are very limited in the literature. Therefore, one may easily show that the numerical methods such as finite element methods (FEM), meshless methods, GDQM, etc. are widely used and have shown great progress for the analysis of these complex problems. However, for convenience and generality considerations at least to the best of the author's knowledge, there is no reported work regarding to the meshless methods of which best fit in terms of accuracy, CPU time, flexibility for dealing with the complex geometries, extendibility to multi-dimensional problems and etc., for the static and dynamic analysis of the two-directional FGBs based on the different beam theories.

Meshless methods are the most promising and have attracted considerable attention for the analysis of engineering problems with intrinsic complexity. Meshless methods are widely used in static and dynamic analyses of the isotropic, laminated composite and FGM beam problems [39–45]. To obtain the approximate solution of the problem by a meshless method, the selection of the basis functions is almost the most important issue. The accuracy of the computed solution can be increased by employing different number of terms in TSE or increasing number of nodes in the problem domain or by increasing the degree of complete polynomials. Many meshless methods have been proposed by researchers to obtain the approximate solution of the problem. The Smoothed Particle Hydrodynamics (SPH) method is proposed by Lucy [46] to the testing of the fission hypothesis. However, this method has two important shortcomings, lack of accuracy on the boundaries and the tensile instability. To remove these shortcomings, many meshless methods have been proposed such as the Corrected Smoothed Particle Method [47–48], Reproducing Kernel Particle Method [49–51], Modified Smoothed Particle Hydrodynamics (MSPH) method [52–56], the Symmetric Smoothed Particle Hydrodynamics method [57–62] and the Strong Form Meshless Implementation of Taylor Series Method [63–64], Moving Kringing Interpolation Method [65–66], the meshless Shepard and Least Squares (MSLS) Method [67], Spectral Meshless Radial Point Interpolation (SMRPI) Method [68].

The main scope of this work is to investigate the static behaviour of the two-directional FGBs based on various beam theories such as EBT, TBT and the Reddy–Bickford Beam Theory (RBT) by using the SSPH method employing the strong formulation.

Based on the above discussions, the main novelty of this work is that there is no reported work on the bending analysis of the two-directional functionally graded beams which are modelled with the power-law variation in 2D based on various beam theories. And also, as far as author is aware there is no work available for static behaviour of the FGBs by using the SSPH method. Further, the SSPH method has an advantage over the MLS, RKPM, MSPH and the SMITSM methods, because basis functions used to approximate the function and its derivatives are derived simultaneously and even a constant weight function can be employed to obtain the approximate solution [57–62].

In Section 2, the formulation of the basis function of the SSPH method is given. In Section 3, the homogenization of material properties of the FGB is presented. The formulation of the EBT, TBT and RBT based on the studied two-directional FGB problems and the SSPH method are given in Section 4. In Section 5, numerical results are given for the problems with four different boundary conditions which are simply supported (SS), clamped-simply supported (CS), clamped-clamped (CC) and clamped-free (CF).

2. Formulation of Symmetric Smoothed Particle Hydrodynamics method

Taylor Series Expansion (TSE) of a scalar function for 1D case can be given by

$$f(\xi) = f(x) + (\xi - x)f'(x) + \frac{1}{2!}(\xi - x)^2 f''(x) + \frac{1}{3!}(\xi - x)^3 f'''(x) + \frac{1}{4!}(\xi - x)^4 f^{(IV)}(x) + \frac{1}{5!}(\xi - x)^5 f^{(V)}(x) + \frac{1}{6!}(\xi - x)^6 f^{(VI)}(x) + \ldots \quad (1)$$

where $f(\xi)$ is the value of the function at ξlocated in near of x. If the zeroth to sixth order terms are employed and the higher order terms are neglected, the Eq. (1) can be written as follows

$$f(\xi) = \boldsymbol{P}(\xi, x)\boldsymbol{Q}(x) \quad (2)$$

where

$$\boldsymbol{Q}(x) = \left[f(x), \frac{df(x)}{dx}, \frac{1}{2!}\frac{d^2 f(x)}{dx^2}, \ldots, \frac{1}{6!}\frac{d^6 f(x)}{dx^6} \right]^T \quad (3)$$

$$\boldsymbol{P}(\xi, x) = [1, (\xi - x), (\xi - x)^2, \ldots, (\xi - x)^6] \quad (4)$$

The number of terms employed in the TSE can be increased to improve the accuracy depending on the order of the governing equations. However, increasing the number of terms to be employed definitely increases the CPU time and may decrease the effectiveness of the method. Determination of the number of terms mainly depends on the experience of the researcher. To determine the unknown variables given in the $\boldsymbol{Q}$(x), both sides of Eq. (2) are multiplied with W$(\xi, \mathrm{x})\boldsymbol{P}(\xi, \mathrm{x})^{\mathrm{T}}$ and evaluated for every node in the CSD. In the global numbering system, let the particle number of the jth particle in the compact support of W(ξ, x) be r (j). The following equation is obtained

$$\sum_{j=1}^{N(x)} f(\xi^{r(j)}) W(\xi^{r(j)}, x) P(\xi^{r(j)}, x)^T \sum_{j=1}^{N(x)} [\boldsymbol{P}(\xi^{r(j)}, x)^T W(\xi^{r(j)}, x)\boldsymbol{P}(\xi^{r(j)}, x)]\boldsymbol{Q}(x) \quad (5)$$

where N(x) is the number nodes in the compact support domain (CSD) of the W(ξ, x) as shown in Fig. 1

Then, Eq. (5) can be given by

$$\boldsymbol{C}(\xi, x)\boldsymbol{Q}(x) = \boldsymbol{D}(\xi, x)\boldsymbol{F}^{(x)}(\xi, x) \quad (6)$$

Where $\boldsymbol{C}(\xi, \mathrm{x}) = \boldsymbol{P}(\xi, \mathrm{x})^{\mathrm{T}}\boldsymbol{W}(\xi, \mathrm{x})\boldsymbol{P}(\xi, \mathrm{x})$ and $\boldsymbol{D}(\xi, \mathrm{x}) = \boldsymbol{P}(\xi, \mathrm{x})^{\mathrm{T}}\boldsymbol{W}(\xi, \mathrm{x})$.

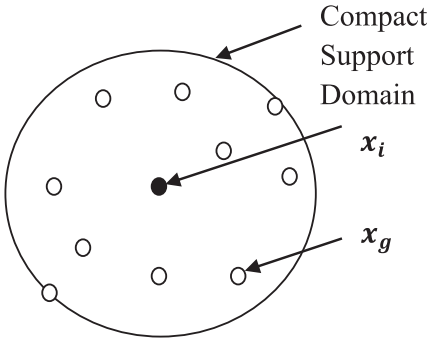

Fig. 1. Compact support of the weight function W(ξ, x) for the node located at $\mathrm{x} = (\mathrm{x_i}, \mathrm{y_i})$.

The solution of Eq. (6) is given by

$$\boldsymbol{Q}(x) = \boldsymbol{K}(\xi, x)\boldsymbol{F}(\xi) \tag{7}$$

where $\boldsymbol{K}^{(x)}(\xi, x) = \boldsymbol{C}(\xi, x)^{-1}\boldsymbol{D}(\xi, x)$. Eq. (7) can be also written as follows

$$Q_I(x) = \sum_{J=1}^{M} K_{IJ}F_J, \quad I = 1, 2, \ldots, 7 \tag{8}$$

where M is the number of nodes and $F_J = f(\xi^J)$. Seven components of Eq. (8) for 1D case are written as

$$\begin{aligned}
f(x) &= Q_1(x) = \sum_{J=1}^{M} K_{1J}F_J \\
\frac{df(x)}{dx} &= Q_2(x) = \sum_{J=1}^{M} K_{2J}F_J \\
\frac{d^2f(x)}{dx^2} &= 2!Q_3(x) = 2!\sum_{J=1}^{M} K_{3J}F_J \\
\frac{d^3f(x)}{dx^3} &= 3!Q_4(x) = 3!\sum_{J=1}^{M} K_{4J}F_J \\
\frac{d^4f(x)}{dx^4} &= 4!Q_5(x) = 4!\sum_{J=1}^{M} K_{5J}F_J \\
\frac{d^5f(x)}{dx^5} &= 5!Q_5(x) = 5!\sum_{J=1}^{M} K_{6J}F_J \\
\frac{d^6f(x)}{dx^6} &= 6!Q_6(x) = 6!\sum_{J=1}^{M} K_{7J}F_J
\end{aligned} \tag{9}$$

Details of the SSPH method can be found in [57–62].

3. Homogenization of material properties

We assume that the two-directional functionally graded beam of length L, width b, thickness h is made of two different constituents. Further, the material properties vary not only in z direction (thickness direction) but also in x direction (along the length of the beam) as shown in Fig. 2.

The rule of mixture is used to find the effective material properties ar a point. According to the rule of mixtures, the effective material properties of the beam, Young's modulus E and shear modulus G can be given by

$$\begin{aligned}
E(x, z) &= E_1V_1(x, z) + E_2V_2(x, z) \\
G(x, z) &= G_1V_1(x, z) + G_2V_2(x, z)
\end{aligned} \tag{10}$$

where E_1, E_2, G_1 and G_2 are the material properties of two constituents, V_1 and $V_2$are volume fractions of the constituents. The relation of the volume fractions can be expressed as follows;

$$V_1(x, z) + V_2(x, z) = 1 \tag{11}$$

According to the power law form, the volume fraction of the constitute 1 can be given by

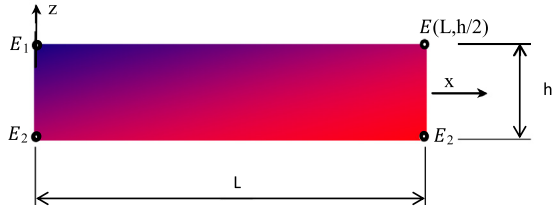

Fig. 2. The variation of elasticity modulus in a two-directional FGB.

$$V_1(x, z) = \left(1 - \frac{x}{2L}\right)^{p_x}\left(\frac{1}{2} + \frac{z}{h}\right)^{p_z} \tag{12}$$

where p_x and p_z are the gradation exponents (power-law index) which determine the material properties through the thickness and length of the beam, respectively. When the p_x and p_z are set to zero the beam becomes homogeneous. The effective material properties can be found by using the Eqs. (10), (11) and (12) as follows

$$\begin{aligned}
E(x, z) &= (E_1 - E_2)\left(1 - \frac{x}{2L}\right)^{p_x}\left(\frac{1}{2} + \frac{z}{h}\right)^{p_z} + E_2 \\
G(x, z) &= (G_1 - G_2)\left(1 - \frac{x}{2L}\right)^{p_x}\left(\frac{1}{2} + \frac{z}{h}\right)^{p_z} + G_2
\end{aligned} \tag{13}$$

4. Formulation of beam theories

The kinematics of deformation of a beam can be represented by using various beam theories. Among them, the Euler Bernoulli Beam Theory (EBT), the Timoshenko Beam Theory (TBT) and the Reddy-Bickford Beam Theory (RBT) are commonly used. The effect of the transverse shear deformation neglected in the EBT is allowed in the latter two beam theories.

Euler Bernoulli beam theory is the simplest beam theory and assumes that the cross sections which are normal to the mid-plane before deformation remain plane/straight and normal to the mid-plane after deformation. Both transverse shear and transverse normal strains are neglected by using these assumptions. In the TBT, the normality assumption of the EBT is relaxed and the cross sections do not need to normal to the mid-plane but still remain plane. The TBT requires the shear correction factor (SCF) to compensate the error due to the assumption of the constant transverse shear strain and shear stress through the beam thickness. The SCF depends on the geometric and material parameters of the beam but the loading and boundary conditions are also important to determine the SCF [68,69]. In the third order shear deformation theory which is named as the RBT, the transverse shear strain is quadratic trough the thickness of the beam [70].

The need for the further extension of the EBT is raised for the engineering applications of the beam problems often characterized by high ratios, up to 40 for the composite structures, between the Young modulus and the shear modulus [71]. Various higher order beam theories are introduced in which the straightness assumption is removed and the vanishing of shear stress at the upper and lower surfaces are accomodated. For this purpose, higher order polynomials incorporating either one, or more, extra terms [72–78] or trigonometric functions [79,80] or exponential functions [81] are included in the expansion of the longitudinal point-wise displacement component through the thickness of the beam. The higher order theories introduce additional unknowns that make the governing equations more complicated and provide the solutions much costly in terms of CPU time. The theories which are higher than the third order shear deformation beam theory are seldom used because the accuracy gained by these theories which require much effort to solve the governing equations is so little [70].

To describe the EBT, TBT and RBT, the following coordinate system is introduced. The x-cordinate is taken along the axis of the beam and the z-coordinate is taken through the height (thickness) of the beam. In the general beam theory, all the loads and the displacements (u,w) along the coordinates (x,z) are only the functions of the x and z coordinates [70]. The formulations of the EBT, TBT and RBT based on the FGM and the SSPH formulations are given below.

4.1. Euler Bernoulli beam theory

The following displacement field is given for the EBT,

$$u(x,z) = -z\frac{dw_0}{dx}$$
$$w(x,z) = w_0(x) \tag{14}$$

where w_0 is the transverse deflection of the point (x,0) which is on the mid-plane (z = 0) of the beam. By using the assumption of the smallness of strains and rotations, the only the axial strain which is nonzero is given by,

$$\varepsilon_{xx} = \frac{du}{dx} = -z\frac{d^2w_0}{dx^2} \tag{15}$$

The virtual strain energy of the beam in terms of the axial stress and the axial strain can be expressed by

$$\delta U = \int_0^L \int_A \sigma_{xx}\delta\varepsilon_{xx} dA dx \tag{16}$$

where δ is the variational operator, A is the cross sectional area, L is the length of the beam, σ_{xx} is the axial stress. The bending moment of the EBT is given by,

$$M_{xx} = \int_A z\sigma_{xx} dA \tag{17}$$

By using Eq. (15) and Eq. (17), Eq. (16) can be rewritten as,

$$\delta U = -\int_0^L M_{xx} z\frac{d^2\delta w_0}{dx^2} \tag{18}$$

The virtual potential energy of the load q(x) which acts at the centre axis of the beam is given by

$$\delta V = -\int_0^L q(x)\delta w_0 dx \tag{19}$$

If a body is in equilibrium, $\delta W = \delta U + \delta V$, the total virtual work (δW) done equals zero. Then one can obtain,

$$\delta W = -\int_0^L \left(M_{xx} z\frac{d^2\delta w_0}{dx^2} + q(x)\delta w_0\right) dx = 0 \tag{20}$$

After performing integration for the first term in Eq. (20) twice and since δw_0 is arbitrary in (0 < x < L), one can obtain following equilibrium equation

$$-\frac{d^2M_{xx}}{dx^2} = q(x) \quad for\ 0 < x < L \tag{21}$$

By introducing the shear force Q_x and rewrite the Eq. (21) in the following form

$$-\frac{dM_{xx}}{dx} + Q_x = 0, -\frac{dQ_x}{dx} = q(x) \tag{22}$$

By using Hooke's law, one can obtain

$$\sigma_{xx} = E(x,z)\varepsilon_{xx} = -\left[(E_1 - E_2)\left(1 - \frac{x}{2L}\right)^{p_x}\left(\frac{1}{2} + \frac{z}{h}\right)^{p_z} + E_2\right] z\frac{d^2w_0}{dx^2} \tag{23}$$

If the Eq. (23) is put into the Eq. (17), it is obtained,

$$M_{xx} = -\int_{-h/2}^{+h/2}\left[(E_1 - E_2)\left(1 - \frac{x}{2L}\right)^{p_x}\left(\frac{1}{2} + \frac{z}{h}\right)^{p_z} + E_2\right] z^2\frac{d^2w_0}{dx^2} dz = -D_{xx}\frac{d^2w_0}{dx^2} \tag{24}$$

where

$$D_{xx} = \int_{-h/2}^{+h/2}\left[(E_1 - E_2)\left(1 - \frac{x}{2L}\right)^{p_x}\left(\frac{1}{2} + \frac{z}{h}\right)^{p_z} + E_2\right] z^2 dz \tag{25}$$

The EBT governing equation for a FGB subjected to the distributed load is given by

$$\frac{d^2}{dx^2}\left(D_{xx}\frac{d^2w_0}{dx^2}\right) = q(x) \quad for\ 0 < x < L \tag{26}$$

4.2. Timoshenko beam theory

The following displacement field is given for the TBT,

$$u(x,z) = z\phi(x)$$
$$w(x,z) = w_0(x) \tag{27}$$

where $\phi(x)$ is the rotation of the cross section. By using the Eq. (27), the strain-displacement relations are given by

$$\varepsilon_{xx} = \frac{du}{dx} = z\frac{d\phi}{dx}$$
$$\gamma_{xz} = \frac{du}{dz} + \frac{dw}{dx} = \phi + \frac{dw_0}{dx} \tag{28}$$

The virtual strain energy of the beam including the virtual energy associated with the shearing strain can be written as,

$$\delta U = \int_0^L \int_A (\sigma_{xx}\delta\varepsilon_{xx} + \sigma_{xz}\delta\gamma_{xz}) dA dx \tag{29}$$

where σ_{xz} is the transverse shear stress and γ_{xz} is the shear strain. The bending moment and the shear force can be written respectively

$$M_{xx} = \int_A z\sigma_{xx} dA, Q_x = \int_A \sigma_{xz} dA \tag{30}$$

By using Eq. (28) and Eq. (30), one can rewrite the Eq. (29) as,

$$\delta U = \int_0^L \left[M_{xx}\frac{d\delta\phi}{dx} + Q_x\left(\delta\phi + \frac{d\delta w_0}{dx}\right)\right] dx \tag{31}$$

The virtual potential energy of the load q(x) which acts at the centre axis of the Timoshenko beam is given by

$$\delta V = -\int_0^L q(x)\delta w_0 dx \tag{32}$$

Since the total virtual work done equals zero and the coefficients of $\delta\phi$ and δw_0in $0 < x < L$ are zero, one can obtain the following equations

$$-\frac{dM_{xx}}{dx} + Q_x = 0, \quad -\frac{dQ_x}{dx} = q(x) \tag{33}$$

The constitute equations can be written as follows

$$\sigma_{xx} = E(x,z)\varepsilon_{xx} = \left[(E_1 - E_2)\left(1 - \frac{x}{2L}\right)^{p_x}\left(\frac{1}{2} + \frac{z}{h}\right)^{p_z} + E_2\right] z\frac{d\phi}{dx} \tag{34}$$

$$\sigma_{xz} = G(x,z)\gamma_{xz} = \left[(G_1 - G_2)\left(1 - \frac{x}{2L}\right)^{p_x}\left(\frac{1}{2} + \frac{z}{h}\right)^{p_z} + G_2\right]\left(\phi + \frac{dw_0}{dx}\right) \tag{35}$$

The bending moment and shear force can be expressed in terms of generalized displacement (w_0, ϕ) by using the constitute equations given above

$$M_{xx}=\int_{-h/2}^{+h/2} z\sigma_{xx}dz=\int_{-h/2}^{+h/2}\left[(E_1-E_2)\left(1-\frac{x}{2L}\right)^{p_x}\left(\frac{1}{2}+\frac{z}{h}\right)^{p_z}+E_2\right]z^2\frac{d\phi}{dx}dz=D_{xx}\frac{d\phi}{dx}$$
$$Q_x=\kappa_s\int_{-\frac{h}{2}}^{+\frac{h}{2}}\sigma_{xz}dz=\kappa_s\int_{-\frac{h}{2}}^{+\frac{h}{2}}\left[(G_1-G_2)\left(1-\frac{x}{2L}\right)^{p_x}\left(\frac{1}{2}+\frac{z}{h}\right)^{p_z}+G_2\right]\left(\phi+\frac{dw_0}{dx}\right)dz$$
$$=\kappa_s A_{xz}\left(\phi+\frac{dw_0}{dx}\right) \tag{36}$$

where κ_s is the shear correction factor to be used to compensate the error caused by the assumption of a constant transverse shear stress distribution along the beam thickness and

$$D_{xx}=\int_{-h/2}^{+h/2}\left[(E_1-E_2)\left(\frac{1}{2}+\frac{x}{L}\right)^{p_x}\left(\frac{1}{2}+\frac{z}{h}\right)^{p_z}+E_2\right]z^2dz$$
$$A_{xz}=\int_{-\frac{h}{2}}^{+\frac{h}{2}}\left[(G_1-G_2)\left(\frac{1}{2}+\frac{x}{L}\right)^{p_x}\left(\frac{1}{2}+\frac{z}{h}\right)^{p_z}+G_2\right]dz \tag{37}$$

The governing equations of the TBT is obtained in terms of generalized displacements as follows

$$-\frac{d}{dx}\left(D_{xx}\frac{d\phi}{dx}\right)+\kappa_s A_{xz}\left(\phi+\frac{dw_0}{dx}\right)=0 \tag{38}$$

$$-\frac{d}{dx}\left[\kappa_s A_{xz}\left(\phi+\frac{dw_0}{dx}\right)\right]=q(x) \tag{39}$$

4.3. Reddy-Bickford beam theory

The following displacement field is given for the RBT,

$$u(x,z)=z\phi(x)-\alpha z^3\left(\phi(x)+\frac{dw(x)}{dx}\right)$$
$$w(x,z)=w_0(x) \tag{40}$$

where $\alpha=4/(3h^2)$. By using the Eq. (40), the strain-displacement relations of the RBT are given by

$$\varepsilon_{xx}=\frac{du}{dx}=z\frac{d\phi}{dx}-\alpha z^3\left(\frac{d\phi}{dx}+\frac{d^2w_0}{dx^2}\right)$$
$$\gamma_{xz}=\frac{du}{dz}+\frac{dw}{dx}=\phi+\frac{dw_0}{dx}-\beta z^2\left(\phi+\frac{dw_0}{dx}\right) \tag{41}$$

where $\beta=3\alpha=4/(h^2)$.

The virtual strain energy of the beam can be written as,

$$\delta U=\int_0^L\int_A(\sigma_{xx}\delta\varepsilon_{xx}+\sigma_{xz}\delta\gamma_{xz})dAdx \tag{42}$$

The usual bending moment and the shear force

$$M_{xx}=\int_A z\sigma_{xx}dA, Q_x=\int_A\sigma_{xz}dA \tag{43}$$

and P_{xx} and R_x are the higher order stress resultants can be written respectively

$$P_{xx}=\int_A z^3\sigma_{xx}dA, R_x=\int_A z^2\sigma_{xz}dA \tag{44}$$

By using Eq. (41), Eq. (43) and Eq. (44) one can rewrite the Eq. (42) as,

$$\delta U=\int_0^L\left[(M_{xx}-\alpha P_{xx})\frac{d\delta\phi}{dx}-\alpha P_{xx}\frac{d^2\delta w_0}{dx^2}+(Q_x-\beta R_x)\left(\delta\phi+\frac{d\delta w_0}{dx}\right)\right]dx \tag{45}$$

In the RBT there is no need to use a SCF unlike the TBT. The virtual potential energy of the transverse load $q(x)$ is given by

$$\delta V=-\int_0^L q(x)\delta w_0dx \tag{46}$$

The constituve equations can be written as follows

$$\sigma_{xx}=E(x,z)\varepsilon_{xx}$$
$$=\left[(E_1-E_2)\left(1-\frac{x}{2L}\right)^{p_x}\left(\frac{1}{2}+\frac{z}{h}\right)^{p_z}+E_2\right]\left[z\frac{d\phi}{dx}-\alpha z^3\left(\frac{d\phi}{dx}+\frac{d^2w_0}{dx^2}\right)\right]$$

$$\sigma_{xz}=G(x,z)\gamma_{xz}$$
$$=\left[(G_1-G_2)\left(1-\frac{x}{2L}\right)^{p_x}\left(\frac{1}{2}+\frac{z}{h}\right)^{p_z}+G_2\right]\left[\phi+\frac{dw_0}{dx}-\beta z^2(\phi+\frac{dw_0}{dx})\right]$$

The governing equations of the RBT are obtained in terms of displacements ϕ and w_0 as follows,

$$-\frac{d}{dx}\left(\bar{D}_{xx}\frac{d\phi}{dx}-\alpha\hat{F}_{xx}\frac{d^2w_0}{dx^2}\right)+\hat{A}_{xz}\left(\phi+\frac{dw_0}{dx}\right)=0 \tag{47}$$

$$-\alpha\frac{d^2}{dx^2}\left(\hat{F}_{xx}\frac{d\phi}{dx}-\alpha H_{xx}\frac{d^2w_0}{dx^2}\right)-\frac{d}{dx}\left[\hat{A}_{xz}(\phi+\frac{dw_0}{dx})\right]=q(x) \tag{48}$$

where

$$\hat{A}_{xz}=\hat{A}_{xz}-\beta\hat{D}_{xz}, \bar{D}_{xx}=\hat{D}_{xx}-\alpha\hat{F}_{xx}$$
$$\hat{D}_{xx}=D_{xx}-\alpha F_{xx}, \hat{F}_{xx}=F_{xx}-\alpha H_{xx}$$
$$\hat{A}_{xz}=A_{xz}-\beta D_{xz}, \hat{D}_{xz}=D_{xz}-\beta F_{xz}$$
$$(D_{xx},F_{xx},H_{xx})=\int_{-h/2}^{+h/2}\left[(E_1-E_2)(1-\tfrac{x}{2L})^{p_x}(\tfrac{1}{2}+\tfrac{z}{h})^{p_z}+E_2\right](z^2,z^4,z^6)dz$$
$$(A_{xz},D_{xz},F_{xz})=\int_{-h/2}^{+h/2}\left[(G_1-G_2)(1-\tfrac{x}{2L})^{p_x}(\tfrac{1}{2}+\tfrac{z}{h})^{p_z}+G_2\right](1,z^2,z^4)dz \tag{49}$$

4.4. Representation of the governing equations by the SSPH method

Based on the EBT, the governing equation of the problem can be presented as algebraic equations by using the SSPH basis function given in Eq. (9) and replacing $f(x)$ with $w_0(x)$ as follows,

$$D_{xx,xx}\sum_{J=1}^{M}2K_{3J}W_J+D_{xx,x}\sum_{J=1}^{M}12K_{4J}W_J+D_{xx}\sum_{J=1}^{M}24K_{5J}W_J$$
$$=q_0\quad for\ 0<x<L \tag{50}$$

where $D_{xx,xx}=\frac{d^2D_{xx}}{dx^2}$ and $D_{xx,x}=\frac{dD_{xx}}{dx}$.

The governing equations of the problem based on the TBT can be written in a similar way by replacing $f(x)$ given in Eq. (9) with $w_0(x)$ and $\phi(x)$ and by using the SSPH basis functions as follows,

$$\sum_{J=1}^{M}\kappa_s A_{xz}K_{2J}W_J+\sum_{J=1}^{M}[\kappa_s A_{xz}K_{1J}-D_{xx,x}K_{2J}-2D_{xx}K_{3J}]\Phi_J=0 \tag{51}$$

$$-\sum_{J=1}^{M}[\kappa_s A_{xz,x}K_{2J}+2\kappa_s A_{xz}K_{3J}]W_J-\sum_{J=1}^{M}[\kappa_s A_{xz,x}K_{1J}+\kappa_s A_{xz}K_{2J}]\Phi_J=q_0 \tag{52}$$

where $A_{xz,x}=\frac{dA_{xz}}{dx}$. The SCF is assumed to be constant as $\kappa_s=5/6$ for the rectangular cross section,

By using RBT and the SSPH basis function the governing equations can be written by replacing $f(x)$ given in Eq. (9) with $w_0(x)$ and $\phi(x)$ as follows,

$$\sum_{J=1}^{M}[\hat{A}_{xz}K_{2J}+2\alpha\hat{F}_{xx,x}K_{3J}+6\alpha\hat{F}_{xx}K_{4J}]W_J+\sum_{J=1}^{M}[\hat{A}_{xz}K_{1J}-\bar{D}_{xx,x}K_{2J}-2\bar{D}_{xx}K_{3J}]\Phi_J=0$$
$$\sum_{J=1}^{M}[-\bar{A}_{xz,x}K_{2J}-2\hat{A}_{xz}K_{3J}+2\alpha^2H_{xx,xx}K_{3J}+12\alpha^2H_{xx,x}K_{4J}+24\alpha^2H_{xx}K_{5J}]W_J$$
$$+\sum_{J=1}^{M}[-\bar{A}_{xz,x}K_{1J}-\hat{A}_{xz}K_{2J}-\alpha\hat{F}_{xx,xx}K_{2J}-4\alpha\hat{F}_{xx,x}K_{3J}-6\alpha\hat{F}_{xx}K_{4J}]\Phi_J=q_0 \tag{53}$$

where $\hat{A}_{xz}=\frac{dA_{xz}}{dx}$, $\hat{F}_{xx,x}=\frac{d\hat{F}_{xx}}{dx}$, $\hat{F}_{xx,xx}=\frac{d^2\hat{F}_{xx}}{dx^2}$, $H_{xx,x}=\frac{dH_{xx}}{dx}$ *and* $H_{xx,xx}=\frac{d^2H_{xx}}{dx^2}$

The SSPH formulation of the boundary conditions for the studied problems is given below.

4.4.1. Simply supported (SS) two-directional FGB

The boundary conditions regarding to the EBT are given as follows;

$$\begin{aligned} &x=0, \sum_{J=1}^{M}2K_{3J}W_J=0 \text{ and } \sum_{J=1}^{M}K_{1J}W_J=0\ m\\ &x=L, \sum_{J=1}^{M}2K_{3J}W_J=0 \text{ and } \sum_{J=1}^{M}K_{1J}W_J=0\ m \end{aligned} \tag{54}$$

The boundary conditions regarding to the TBT are given as follows;

$$\begin{aligned} &x=0, \quad \sum_{J=1}^{M}K_{2J}\Phi_J=0 \text{ and } \sum_{J=1}^{M}K_{1J}W_J=0\ m\\ &x=L, \quad \sum_{J=1}^{M}K_{2J}\Phi_J=0 \text{ and } \sum_{J=1}^{M}K_{1J}W_J=0\ m \end{aligned} \tag{55}$$

The boundary conditions regarding to the TBT are given as follows;

$$\begin{aligned} &x=0, \quad \sum_{J=1}^{M}\hat{D}_{xx}K_{2J}\Phi_J-\sum_{J=1}^{M}2\alpha F_{xx}K_{3J}W_J=0, \text{ and } \sum_{J=1}^{M}K_{1J}W_J=0\ m\\ &x=L, \quad \sum_{J=1}^{M}\hat{D}_{xx}K_{2J}\Phi_J-\sum_{J=1}^{M}2\alpha F_{xx}K_{3J}W_J=0, \text{ and } \sum_{J=1}^{M}K_{1J}W_J=0\ m \end{aligned} \tag{56}$$

4.4.2. Clamped simply supported (CS) two-directional FGB

The boundary conditions based on the EBT are given by;

$$\begin{aligned} &x=0, \quad \sum_{J=1}^{M}K_{2J}W_J=0 \text{ and } \sum_{J=1}^{M}K_{1J}W_J=0\ m\\ &x=L, \quad \sum_{J=1}^{M}2K_{3J}W_J=0 \text{ and } \sum_{J=1}^{M}K_{1J}W_J=0\ m \end{aligned} \tag{57}$$

The boundary conditions based on the TBT are given by;

$$\begin{aligned} &x=0, \quad \sum_{J=1}^{M}K_{1J}\Phi_J=0 \text{ and } \sum_{J=1}^{M}K_{1J}W_J=0\ m\\ &x=L, \quad \sum_{J=1}^{M}K_{2J}\Phi_J=0 \text{ and } \sum_{J=1}^{M}K_{1J}W_J=0\ m \end{aligned} \tag{58}$$

The boundary conditions based on the RBT are given by;

$$\begin{aligned} &x=0, \quad \sum_{J=1}^{M}K_{1J}\Phi_J=0 \text{ and } \sum_{J=1}^{M}K_{1J}W_J=0\ m\\ &x=L, \quad \sum_{J=1}^{M}\hat{D}_{xx}K_{2J}\Phi_J-\sum_{J=1}^{M}2\alpha F_{xx}K_{3J}W_J=0, \quad \text{and } \sum_{J=1}^{M}K_{1J}W_J=0\ m \end{aligned} \tag{59}$$

4.4.3. Clamped clamped (CC) two-directional FGB

The boundary conditions based on the EBT are given by;

$$\begin{aligned} &x=0, \quad \sum_{J=1}^{M}K_{2J}W_J=0 \text{ and } \sum_{J=1}^{M}K_{1J}W_J=0\ m\\ &x=L, \quad \sum_{J=1}^{M}K_{2J}W_J=0 \text{ and } \sum_{J=1}^{M}K_{1J}W_J=0\ m \end{aligned} \tag{60}$$

The boundary conditions based on the TBT are given by;

$$\begin{aligned} &x=0, \quad \sum_{J=1}^{M}K_{1J}\Phi_J=0 \text{ and } \sum_{J=1}^{M}K_{1J}W_J=0\ m\\ &x=L, \quad \sum_{J=1}^{M}K_{1J}\Phi_J=0 \text{ and } \sum_{J=1}^{M}K_{1J}W_J=0\ m \end{aligned} \tag{61}$$

The boundary conditions based on the RBT are given by;

$$\begin{aligned} &x=0, \quad \sum_{J=1}^{M}K_{1J}\Phi_J=0 \text{ and } \sum_{J=1}^{M}K_{1J}W_J=0\ m\\ &x=L, \quad \sum_{J=1}^{M}K_{1J}\Phi_J=0 \text{ and } \sum_{J=1}^{M}K_{1J}W_J=0\ m \end{aligned} \tag{62}$$

4.4.4. Cantilever (CF) two-directional FGB

The boundary conditions based on the EBT are given by;

$$\begin{aligned} &x=0, \quad \sum_{J=1}^{M}K_{2J}W_J=0 \text{ and } \sum_{J=1}^{M}K_{1J}W_J=0\ m\\ &x=L, \quad \sum_{J=1}^{M}2K_{3J}W_J=0 \text{ and } \sum_{J=1}^{M}[2D_{xx,x}K_{3J}+6D_{xx}K_{4J}]W_J=0 \end{aligned} \tag{63}$$

The boundary conditions regarding to the TBT are given as follows;

$$\begin{aligned} &x=0, \quad \sum_{J=1}^{M}K_{1J}\Phi_J=0 \text{ and } \sum_{J=1}^{M}K_{1J}W_J=0\ m\\ &x=L, \quad \sum_{J=1}^{M}K_{2J}\Phi_J=0 \text{ and } \sum_{J=1}^{M}K_{1J}\Phi_J+\sum_{J=1}^{M}K_{2J}W_J=0 \end{aligned} \tag{64}$$

The boundary conditions regarding to the RBT are given as follows;

$$\begin{aligned} &x=0, \quad \sum_{J=1}^{M}K_{1J}\Phi_J=0 \text{ and } \sum_{J=1}^{M}K_{1J}W_J=0\ m\\ &x=L, \quad \sum_{J=1}^{M}\hat{D}_{xx}K_{2J}\Phi_J-\sum_{J=1}^{M}2\alpha F_{xx}K_{3J}W_J=0, \text{ and } \sum_{J=1}^{M}K_{1J}\Phi_J+\sum_{J=1}^{M}K_{2J}W_J=0 \end{aligned} \tag{65}$$

5. Numerical results

The elastostatic behaviour of the FGBs are investigated by using various beam theories which are the EBT, TBT and RBT. The numerical solutions are obtained by using the SSPH method for various gradation exponents, aspect ratios and boundary conditions. Since there is no available previous results for the bending analysis of two-directional FGBs with power law rule, as the first, the developed code is verified by solving a simply supported conventional FGB problem subjected to uniformly distributed load. The computed results are compared with the results from previous studies [82] along with the analytical solutions. The dimensionless maximum transverse deflections, axial and shear stresses are calculated for the comparison purpose. After the verification of the developed

code, the number of nodes to be used in the problem domain for the numerical calculations is determined.

For each problem studied here, the physical parameters of the beam are L = 1 m and b = 0.1 m. Two different two aspect ratios, L/h = 5 and 20, are considered. The distributed load q_0 is set to 10,000 N/m. The material properties of the two constitutes are given as

$$Ceramic\ (Al_2O_3): E_1 = 380\ GPa\ and\ \nu_1 = 0.3$$

$$Metal\ (Aluminium): E_2 = 70\ GPa\ and\ \nu_2 = 0.3$$

The following non-dimensional quantities are used for the representation of the results;

Non-dimensional maximum transverse deflection of the beam:

$$\begin{aligned}\bar{w} &= \frac{100E_2h^3}{q_0L^4}w_0\left(\frac{L}{2},z\right)\ for\ SS, CS\ and\ CC\ beams\\ \bar{w} &= \frac{100E_2h^3}{q_0L^4}w_0(L,z)\ for\ CF\ beam\end{aligned} \tag{66}$$

Non-dimensional axial and shear stresses of the beam:

$$\begin{aligned}\bar{\sigma}_x &= \frac{h}{q_0L}\sigma_x\left(\frac{L}{2},z\right)\\ \bar{\sigma}_{xz} &= \frac{h}{q_0L}\sigma_{xz}(0,z)\end{aligned} \tag{67}$$

5.1. Verification, comparison and convergence studies

To verify the developed code, a simply supported FGB under uniformly distributed load is considered. For numerical calculations to be performed by the SSPH method uniformly distributed 21, 41, 81 and 161 nodes are used in the problem domain $x \in [0,1]$. The Revised Super Gauss Function (RSGF) is employed as a weight (kernel) function.

$$W(x,\xi) = \frac{G}{(h\sqrt{\pi})^{\lambda}}\begin{Bmatrix}(64-d^2)e^{-d^2} & 0 \leqslant d \leqslant 8\\ 0 & d > 8\end{Bmatrix} \quad d = |x-\xi|/h \tag{68}$$

where d is the radius of the CSD, h is the smoothing length. G and λ are the parameters which are eliminated from the both side of the equations by the formulation of the SSPH method.

The numerical calculations are performed according to the following meshless parameters; the radius of the support domain (d) is chosen as 8 and the smoothing length (h) equals to 1.3Δ where Δ is the minimum distance between two adjacent nodes. The meshless parameters, d and h, are selected to obtain the lowest error.

The maximum non-dimensional transverse deflections, axial and shear stresses obtained from different beam theories for various node distributions, aspect ratios and gradation exponents are given in Tables 1–6 along with the results from previous studies and the analytical solution of the problem. It is clear that the results obtained by using the SSPH method agree completely with those of previous paper [82] and the analytical solution. As it is seen in Tables 1–6, the transverse deflections, axial and transverse shear stresses computed by the SSPH method are almost the same with the analytical solutions for the EBT and TBT. The numerical results based on the RBT are compared with the results given in [82] where the analytical solution of a third order beam theory is presented. Tables 1–6 show that the results from RBT are in excellent agreement with the results presented in [82]. Due to this agreement, the verification of the developed code is established. For the studies to be presented below, the number of nodes to be used for the numerical calculations of the problems is determined as 161 for the sake of accuracy.

5.2. Elastostatic analysis of two-directional FGBs

Four different boundary conditions, SS, CS, CC and CF are considered respectively for the bending analysis of two directional FGBs subjected to uniformly distributed load. The maximum transverse deflections, axial and shear stresses are computed based on the various beam theories, gradation exponents and aspect ratios.

5.2.1. SS two-directional FGB

As the first example, simply supported two directional FGB under uniformly distributed load is studied. The maximum dimensionless transverse deflections and stresses are computed from different beam theories for various gradation exponents and aspect ratios. As it is seen form Tables 7 and 8, the minimum deflection value is obtained from the formulation of EBT, as expected. The difference between the EBT and the other two theories is significant for thick beam (L/h = 5), however for thin beam (L/h = 20), it is negligible. The computed results by RBT are slightly higher than the results from TBT. With the increasing of the gradation exponents in both directions, the deflection values are increasing.

Table 1
Verification and convergence studies of the code for S-S FGB, dimensionless maximum transverse deflections for different number of nodes and gradation exponents, L/h = 5.

Theory	Gradation exponent (p_z)	Number of nodes				Analytical solution/*Li et al. [82]
		21	41	81	161	
EBT	0	2.8783	2.8783	2.8783	2.8783	2.8783
	0.5	4.1296	4.1296	4.1296	4.1296	4.1296
	1	4.8611	4.8611	4.8611	4.8611	4.8611
	2	5.6378	5.6378	5.6378	5.6378	5.6378
	5	6.8975	6.8975	6.8975	6.8975	6.8975
TBT	0	3.1657	3.1657	3.1657	3.1657	3.1657
	0.5	4.5243	4.5243	4.5243	4.5243	4.5243
	1	5.3464	5.3464	5.3464	5.3464	5.3464
	2	6.2679	6.2679	6.2679	6.2679	6.2679
	5	7.7951	7.7951	7.7951	7.7951	7.7951
RBT	0	3.1657	3.1657	3.1657	3.1657	*3.1657
	0.5	4.5175	4.5175	4.5175	4.5177	*4.5183
	1	5.3464	5.3464	5.3464	5.3464	*5.3464
	2	6.3109	6.3109	6.3109	6.3109	*6.3002
	5	7.9760	7.9759	7.9760	7.9760	*7.9268

Table 2
Verification and convergence studies of the code for S-S FGB, dimensionless maximum transverse deflections for different number of nodes and gradation exponents, L/h = 20.

Theory	Number of nodes	Number of nodes				Analytical solution/*Li et al. [82]
		21	41	81	161	
EBT	0	2.8783	2.8783	2.8783	2.8783	2.8783
	0.5	4.1296	4.1296	4.1296	4.1296	4.1296
	1	4.8611	4.8611	4.8611	4.8611	4.8611
	2	5.6378	5.6378	5.6378	5.6378	5.6378
	5	6.8975	6.8975	6.8975	6.8975	6.8975
TBT	0	2.8962	2.8962	2.8962	2.8962	2.8962
	0.5	4.1543	4.1543	4.1543	4.1543	4.1543
	1	4.8914	4.8914	4.8914	4.8914	4.8914
	2	5.6773	5.6773	5.6773	5.6773	5.6773
	5	6.9536	6.9536	6.9536	6.9536	6.9536
RBT	0	2.8962	2.8962	2.8962	2.8962	*2.8962
	0.5	4.1538	4.1538	4.1538	4.1538	*4.1539
	1	4.8914	4.8914	4.8914	4.8914	*4.8914
	2	5.6799	5.6799	5.6799	5.6799	*5.6793
	5	6.9649	6.9649	6.9649	6.9649	*6.9619

Table 3
Verification and convergence studies of the code for S-S FGB, dimensionless axial stress $\bar{\sigma}_x(\frac{L}{2},\frac{h}{2})$ for different number of nodes and gradation exponents, L/h = 5.

Theory	Number of nodes	Number of nodes				Analytical solution/*Li et al. [82]
		21	41	81	161	
EBT	0	3.7500	3.7500	3.7500	3.7500	3.7500
	0.5	5.3803	5.3803	5.3803	5.3802	5.3803
	1	6.3333	6.3333	6.3333	6.3333	6.3333
	2	7.3454	7.3454	7.3454	7.3453	7.3454
	5	8.9865	8.9865	8.9865	8.9864	8.9865
TBT	0	3.7500	3.7500	3.7500	3.7500	3.7500
	0.5	5.3803	5.3803	5.3803	5.3803	5.3803
	1	6.3333	6.3333	6.3333	6.3333	6.3333
	2	7.3454	7.3454	7.3454	7.3454	7.3454
	5	8.9865	8.9865	8.9865	8.9865	8.9865
RBT	0	3.8020	3.8020	3.8020	3.8020	*3.8020
	0.5	5.4525	5.4525	5.4525	5.4525	*5.4526
	1	6.4212	6.4212	6.4212	6.4212	*6.4212
	2	7.4601	7.4601	7.4601	7.4601	*7.4583
	5	9.1544	9.1544	9.1544	9.1544	*9.1467

Table 4
Verification and convergence studies of the code for S-S FGB, dimensionless axial stress $\bar{\sigma}_x(\frac{L}{2},\frac{h}{2})$ for different number of nodes and gradation exponents, L/h = 20.

Theory	Number of nodes	Number of nodes				Analytical solution/*Li et al. [82]
		21	41	81	161	
EBT	0	15.0000	15.0000	15.0000	15.0000	15.0000
	0.5	21.5210	21.5210	21.5211	21.5209	21.5210
	1	25.3333	25.3333	25.3334	25.3332	25.3333
	2	29.3814	29.3815	29.3815	29.3813	29.3814
	5	35.9459	35.9460	35.9460	35.9457	35.9459
TBT	0	15.0000	15.0000	15.0000	15.0000	15.0000
	0.5	21.5210	21.5210	21.5211	21.5210	21.5210
	1	25.3333	25.3333	25.3334	25.3332	25.3333
	2	29.3814	29.3815	29.3815	29.3813	29.3814
	5	35.9459	35.9460	35.9460	35.9460	35.9459
RBT	0	15.0130	15.0130	15.0130	15.0130	*15.0130
	0.5	21.5391	21.5391	21.5391	21.5391	*21.5391
	1	25.3553	25.3553	25.3553	25.3553	*25.3553
	2	29.4101	29.4101	29.4101	29.4101	*29.4097
	5	35.9879	35.9879	35.9879	35.9879	*35.9860

In Figs. 3 and 4, the axial and shear stresses for various theories and gradation exponents in z and x directions are plotted, the aspect ratio is set to L/h = 20. It is found that the axial stresses computed for each theory are almost same, the difference is negligible. It is clear that the maximum shear stress increases by increasing of gradation exponent in z direction whereas the maximum axial stress decreases for TBT. However, the same results are not obtained for RBT. When the gradation exponent p_z is set to 5, the

Table 5
Verification and convergence studies of the code for S-S FGB, dimensionless transverse shear stress $\bar{\sigma}_{xz}(0,0)$ for different number of nodes and gradation exponents, L/h = 5.

Theory	Number of nodes	Number of nodes				Analytical solution/*Li et al. [82]
		21	41	81	161	
TBT	0	0.6000	0.6000	0.6000	0.6000	0.6000
	0.5	0.6272	0.6272	0.6272	0.6272	0.6272
	1	0.6000	0.6000	0.6000	0.6000	0.6000
	2	0.5106	0.5106	0.5106	0.5106	0.5106
	5	0.3930	0.3930	0.3930	0.3930	0.3930
RBT	0	0.7500	0.7500	0.7500	0.7500	*0.7500
	0.5	0.7662	0.7662	0.7662	0.7662	*0.7676
	1	0.7500	0.7500	0.7500	0.7500	*0.7500
	2	0.6897	0.6897	0.6897	0.6897	*0.6787
	5	0.6067	0.6067	0.6067	0.6067	*0.5790

Table 6
Verification and convergence studies of the code for S-S FGB, dimensionless transverse shear stress $\bar{\sigma}_{xz}(0,0)$ for different number of nodes and gradation exponents, L/h = 20.

Theory	Number of nodes	Number of nodes				Analytical solution/*Li et al. [82]
		21	41	81	161	
TBT	0	0.6000	0.6000	0.6000	0.6000	0.6000
	1	0.6272	0.6272	0.6272	0.6272	0.6272
	2	0.6000	0.6000	0.6000	0.6000	0.6000
	5	0.5106	0.5106	0.5106	0.5106	0.5106
	10	0.3930	0.3930	0.3930	0.3930	0.3930
RBT	0	0.7500	0.7500	0.7500	0.7500	*0.7500
	1	0.7662	0.7662	0.7662	0.7662	*0.7676
	2	0.7500	0.7500	0.7500	0.7500	*0.7500
	5	0.6897	0.6897	0.6897	0.6897	*0.6787
	10	0.6067	0.6067	0.6067	0.6067	*0.5790

Table 7
Dimensionless maximum transverse deflections of the S-S FGB for different beam theories and gradation exponents, L/h = 5.

Theory	p_z	p_x				
		0	0.5	1	2	5
EBT	0	2.8783	3.2437	3.6487	4.5720	7.8224
	0.5	4.1296	4.5955	5.0960	6.1772	9.4607
	1	4.8611	5.3703	5.977	7.0356	10.2286
	2	5.6378	6.1810	6.7436	7.8916	10.9342
	5	6.8975	7.4699	8.0458	9.1719	11.8976
TBT	0	3.1657	3.5714	4.0238	5.0595	8.6549
	0.5	4.5243	5.0400	5.5961	6.8004	10.3999
	1	5.3464	5.9113	6.5087	7.7623	11.2435
	2	6.2679	6.8719	7.4972	8.7657	12.0524
	5	7.7951	8.4266	9.0584	10.2806	13.1706
RBT	0	3.1658	3.5714	4.0237	5.0596	8.6546
	0.5	4.5177	5.0327	5.5887	6.7924	10.3939
	1	5.3464	5.9110	6.5085	7.7623	11.2433
	2	6.3111	6.9154	7.5397	8.8052	12.0793
	5	7.9761	8.5963	9.2143	10.4114	13.2574

Table 8
Dimensionless maximum transverse deflections of the S-S FGB for different beam theories and gradation exponents, L/h = 20.

Theory	p_z	p_x				
		0	0.5	1	2	5
EBT	0	2.8783	3.2437	3.6487	4.5720	7.8224
	0.5	4.1296	4.5955	5.0960	6.1772	9.4607
	1	4.8611	5.3703	5.977	7.0356	10.2286
	2	5.6378	6.1810	6.7436	7.8916	10.9342
	5	6.8975	7.4699	8.0458	9.1719	11.8976
TBT	0	2.8963	3.2642	3.6721	4.6024	7.8742
	0.5	4.1543	4.6232	5.1272	6.2161	9.5193
	1	4.8915	5.4041	5.9452	7.0809	10.2919
	2	5.6773	6.2241	6.7907	7.9462	11.0038
	5	6.9536	7.5296	8.1090	9.2412	11.9770
RBT	0	2.8962	3.2641	3.6721	4.6023	7.8742
	0.5	4.1538	4.6228	5.1267	6.2156	9.5189
	1	4.8914	5.4041	5.9452	7.0808	10.2918
	2	5.6799	6.2268	6.7933	7.9486	11.0055
	5	6.9649	7.5402	8.1187	9.2493	11.9824

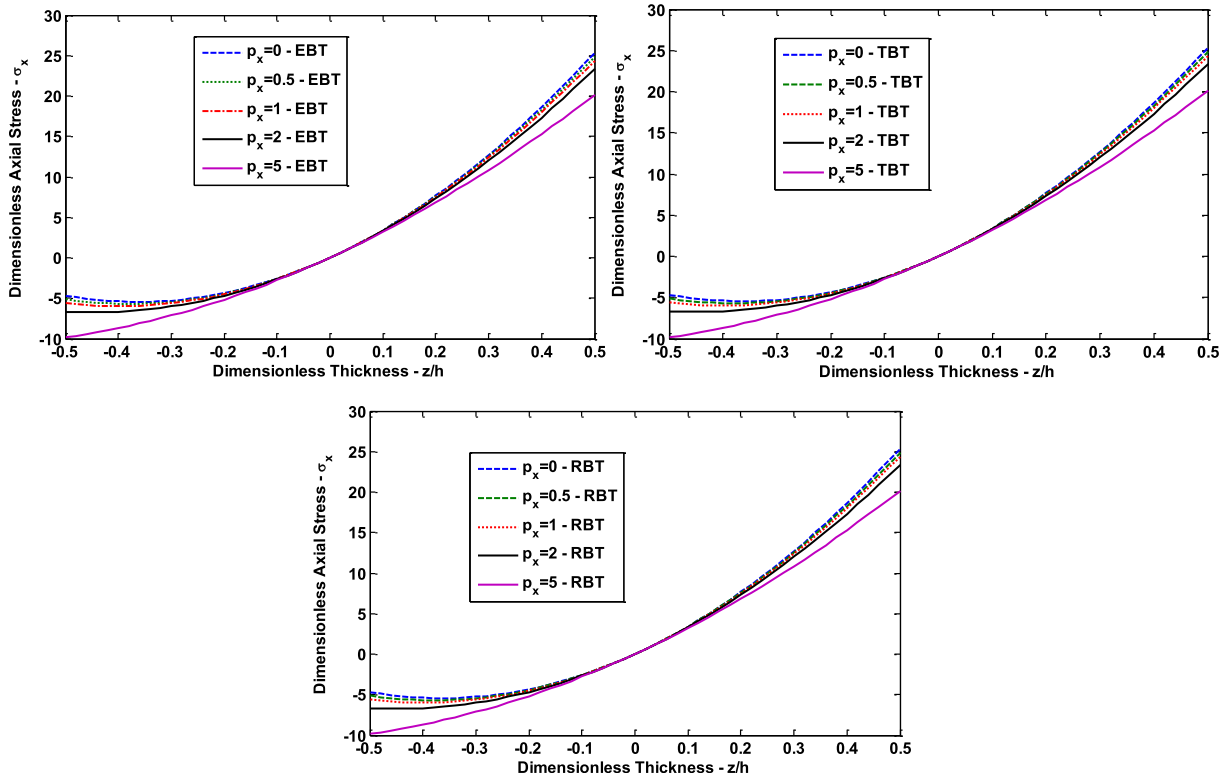

Fig. 3. Dimensionless axial stress $\bar{\sigma}_x\left(\frac{L}{2}, z\right)$ through the thickness of the S-S FGB for different beam theories and $p_z = 1$, L/h = 20.

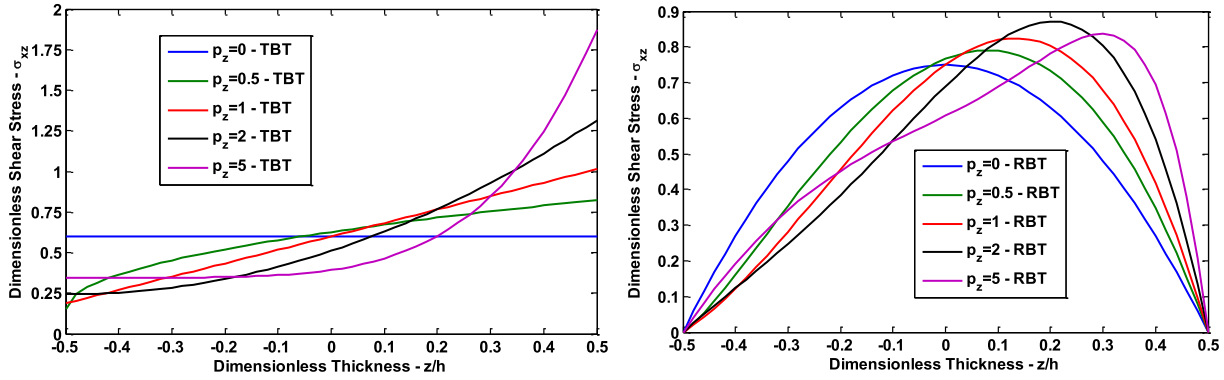

Fig. 4. Dimensionless transverse shear stress $\bar{\sigma}_{xz}(0, z)$ through the thickness of the S-S FGB for different beam theories and $p_x = 1$, L/h = 20.

Table 9
Dimensionless maximum transverse deflections of the C-S FGB for different beam theories and gradation exponents, L/h = 5.

Theory	p_z	p_x				
		0	0.5	1	2	5
EBT	0	1.1972	1.3301	1.4733	1.7845	2.7279
	0.5	1.7176	1.8872	2.0643	2.4296	3.3975
	1	2.0219	2.2072	2.3975	2.7791	3.7281
	2	2.3450	2.5426	2.7419	3.1311	4.0432
	5	2.8689	3.0772	3.2817	3.6642	4.4918
TBT	0	1.5275	1.6915	1.8695	2.2591	3.4454
	0.5	2.1713	2.3794	2.5980	3.0524	4.2647
	1	2.5797	2.8082	3.0440	3.5191	4.7064
	2	3.0691	3.3145	3.5624	4.0457	5.1784
	5	3.9005	4.1567	4.4065	4.8710	5.8706
RBT	0	1.5883	1.7549	1.9357	2.3312	3.5308
	0.5	2.2436	2.4542	2.6758	3.1360	4.3615
	1	2.6823	2.9146	3.1540	3.6363	4.8378
	2	3.2683	3.5193	3.7722	4.2632	5.4062
	5	4.3637	4.6197	4.8680	5.3283	6.3107

maximum shear stress is lower than the stress obtained for the one obtained by $p_z = 2$. As it is expected, the shear stress is zero at the top and the bottom surface of the beam for RBT.

5.2.2. CS two-directional FGB

In this example, the static behaviour of a clamped-simply supported two directional FGB under uniformly distributed load is considered. The results are given in Tables 9 and 10 and Figs. 5 and 6 for different beam theories, gradation exponents and aspect ratios. It is clear from Tables 9 and 10 that, the EBT underestimates the transverse deflections for a thick beam, as expected it acts more stiff than the other two beam models. However, for a thin beam (L/h = 20), the difference is negligible. The computed results by RBT are again slightly higher than the results from TBT. As the gradation exponents in both directions increase, the transverse deflections increase.

The axial and shear stresses for various theories and gradation exponents in z and x directions are given in Figs. 5 and 6, as the aspect ratio is set to L/h = 20. Again, it is observed that the computed axial stresses are almost same for each beam theory. The differences in terms of computed results can be ignored. As gradation exponent in x direction increases the maximum axial stress

Table 10
Dimensionless maximum transverse deflections of the C-S FGB for different beam theories and gradation exponents, L/h = 20.

Theory	p_z	p_x				
		0	0.5	1	2	5
EBT	0	1.1972	1.3301	1.4733	1.7845	2.7279
	0.5	1.7176	1.8872	2.0643	2.4296	3.3975
	1	2.0219	2.2072	2.3975	2.7791	3.7281
	2	2.3450	2.5426	2.7419	3.1311	4.0432
	5	2.8689	3.0772	3.2817	3.6642	4.4918
TBT	0	1.2178	1.3527	1.4981	1.8142	2.7728
	0.5	1.7460	1.9179	2.0977	2.4686	3.4518
	1	2.0568	2.2447	2.4376	2.8254	3.7894
	2	2.3903	2.5908	2.7932	3.1883	4.1142
	5	2.9334	3.1448	3.3520	3.7398	4.5779
RBT	0	1.2217	1.3568	1.5023	1.8187	2.7782
	0.5	1.7506	1.9227	2.1026	2.4739	3.4580
	1	2.0634	2.2515	2.4449	2.8329	3.7978
	2	2.4030	2.6039	2.8066	3.2021	4.1287
	5	2.9631	3.1744	3.3815	3.7689	4.6059

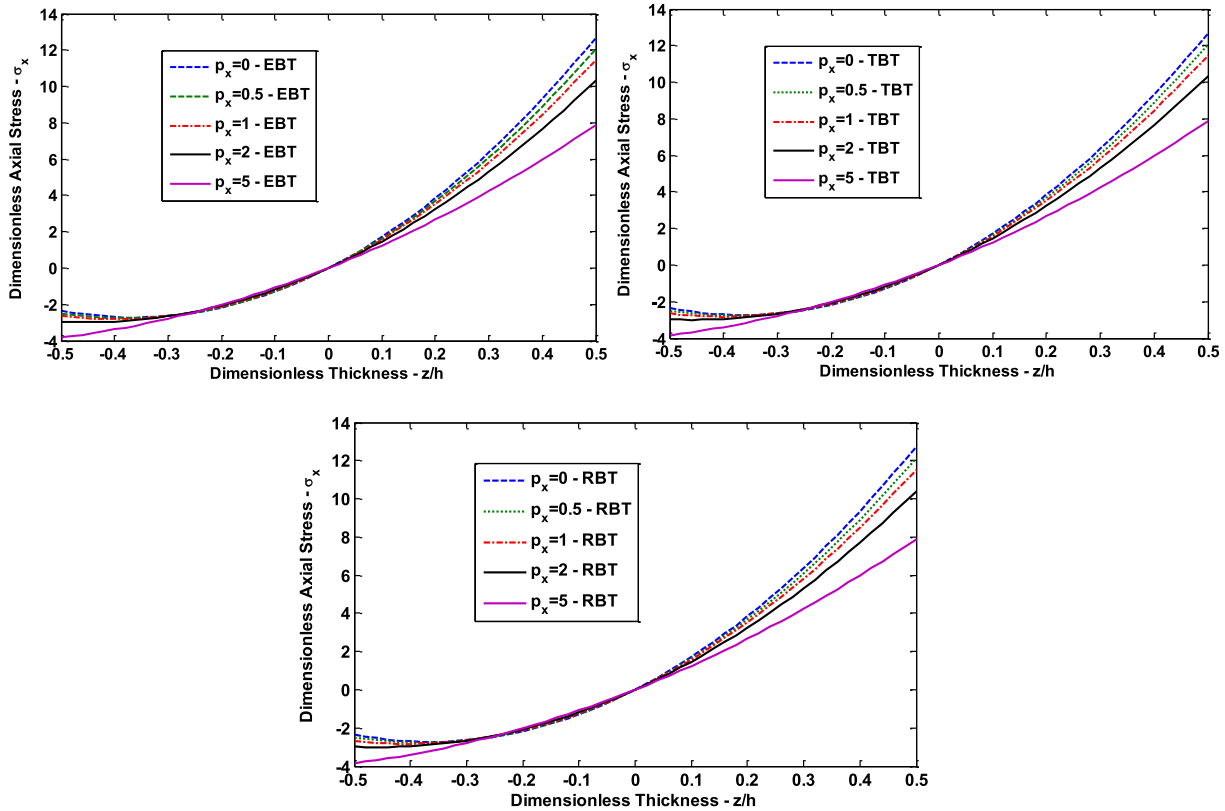

Fig. 5. Dimensionless axial stress $\bar{\sigma}_x\left(\frac{L}{2}, z\right)$ through the thickness of the C-S FGB for different beam theories and $p_z = 1$, L/h = 20.

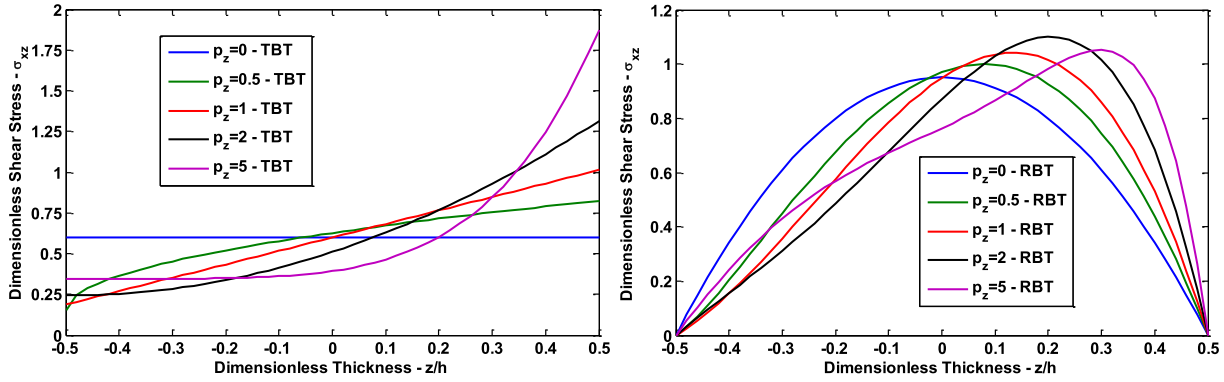

Fig. 6. Dimensionless transverse shear stress $\bar{\sigma}_{xz}(0,z)$ through the thickness of the C-S FGB for different beam theories and $p_x = 1$, L/h = 20.

Table 11
Dimensionless maximum transverse deflections of the C-C FGB for different beam theories and gradation exponents, L/h = 5.

Theory	p_z	p_x				
		0	0.5	1	2	5
EBT	0	0.5757	0.6526	0.7352	0.9111	1.4013
	0.5	0.8259	0.9238	1.0250	1.2279	1.7179
	1	0.9722	1.0791	1.1871	1.3972	1.8722
	2	1.1276	1.2414	1.3541	1.5664	2.0180
	5	1.3795	1.4992	1.6139	1.8199	2.2239
TBT	0	0.8630	0.9793	1.1054	1.3781	2.1431
	0.5	1.2206	1.2206	1.5203	1.8316	2.5887
	1	1.4576	1.4576	1.7832	2.1056	2.8313
	2	1.7576	1.7576	2.1029	2.4249	3.0947
	5	2.2770	2.2770	2.6228	2.9182	3.4756
RBT	0	0.9349	1.0616	1.1988	1.4952	2.3135
	0.5	1.3081	1.4666	1.6324	1.9694	2.7793
	1	1.5789	1.5789	1.9332	2.2820	3.0541
	2	1.9786	1.9786	2.3546	2.6978	3.3912
	5	2.7652	2.7652	3.1075	3.3916	3.9198

Table 12
Dimensionless maximum transverse deflections of the C-C FGB for different beam theories and gradation exponents, L/h = 20.

Theory	p_z	p_x				
		0	0.5	1	2	5
EBT	0	0.5757	0.6526	0.7352	0.9111	1.4013
	0.5	0.8259	0.9238	1.0250	1.2279	1.7179
	1	0.9722	1.0791	1.1871	1.3972	1.8722
	2	1.1276	1.2414	1.3541	1.5664	2.0180
	5	1.3795	1.4992	1.6139	1.8199	2.2239
TBT	0	0.5936	0.6731	0.7583	0.9403	1.4477
	0.5	0.8506	0.9515	1.0559	1.2656	1.7724
	1	1.0003	1.1128	1.2244	1.4415	1.9322
	2	1.1670	1.2845	1.4009	1.6200	2.0854
	5	1.4356	1.5589	1.6770	1.8886	2.3022
RBT	0	0.5981	0.6782	0.7642	0.9477	1.4586
	0.5	0.8561	0.9577	1.0629	1.2743	1.7845
	1	1.0101	1.1213	1.2338	1.4526	1.9463
	2	1.1808	1.2993	1.4166	1.6371	2.1040
	5	1.4661	1.5894	1.7072	1.9182	2.3299

decreases. It is found that the maximum shear stress value is obtained based on TBT for $p_z = 5$, however RBT yields the maximum for $p_z = 2$.

5.2.3. CC two-directional FGB

The dimensionless maximum transverse deflections and the axial and shear stresses of the clamped-clamped FGB are investigated in the third example. The computed results are given in Tables 11 and 12 and Figs. 7 and 8. It is clear in that the transverse deflections increase as the power low index increases. When the RBT and TBT are employed, the difference is significant for the aspect ratio which is set to L/h = 5.

In Figs. 7 and 8, the axial and shear stresses for various theories and gradation exponents in z and directions are given for a clamped-clamped FGB where the aspect ratio is set to L/h = 20. It is found that the computed axial and shear stresses are almost

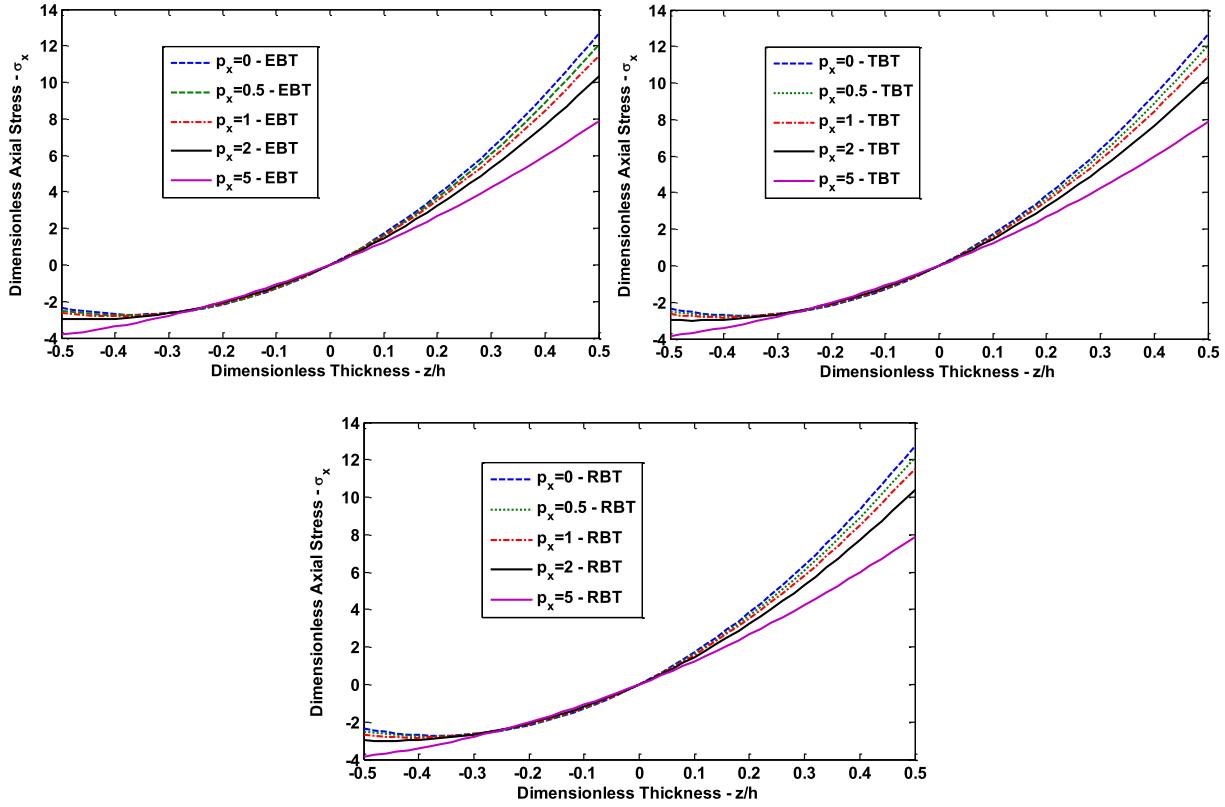

Fig. 7. Dimensionless axial stress $\bar{\sigma}_x(\frac{L}{2},z)$ through the thickness of the C-C FGB for different beam theories and $p_z = 1$, L/h = 20.

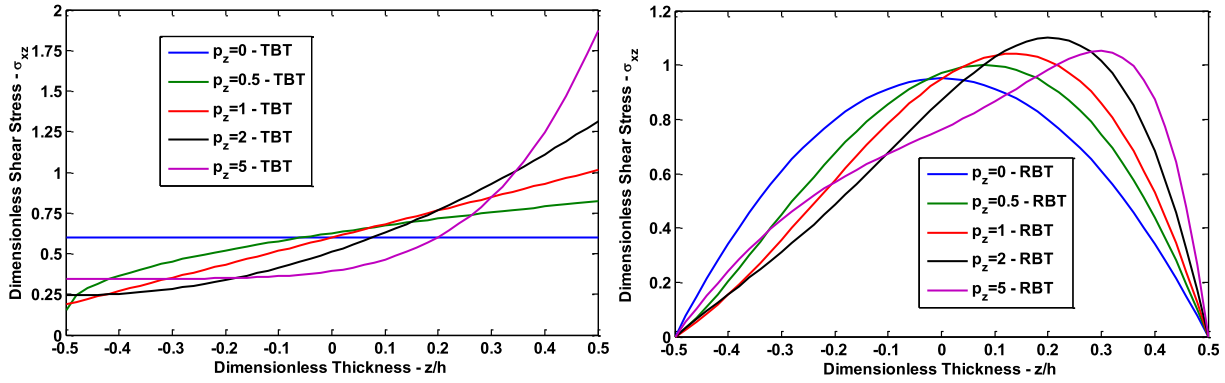

Fig. 8. Dimensionless transverse shear stress $\bar{\sigma}_{xz}(0,z)$ through the thickness of the C-C FGB for different beam theories and $p_x = 1$, L/h = 20.

Table 13
Dimensionless maximum transverse deflections of the C-F FGB for different beam theories and gradation exponents, L/h = 5.

Theory	p_z	p_x				
		0	0.5	1	2	5
EBT	0	27.6324	28.9040	30.2570	33.1881	43.3767
	0.5	39.6381	41.2764	42.9833	46.5753	58.0487
	1	46.6597	48.4570	50.3113	54.1526	65.9210
	2	54.1156	56.0402	58.0056	62.0128	73.8132
	5	66.2063	68.2476	70.2990	74.3814	85.7472
TBT	0	28.7811	30.1520	31.6085	34.7720	45.7606
	0.5	41.2228	42.9784	44.8109	48.6733	60.9781
	1	48.6080	50.5371	52.5297	56.6592	69.2494
	2	56.6437	58.7142	60.8281	65.1309	77.6954
	5	69.8064	71.9918	74.1824	78.5227	90.4724
RBT	0	29.3220	30.6968	32.1525	35.3590	46.4132
	0.5	41.9632	43.8175	45.5368	49.4849	61.7540
	1	49.5423	51.4136	53.4684	57.5021	70.1904
	2	58.1429	60.2877	62.3212	66.7952	79.2699
	5	72.9688	75.2389	77.1708	81.4229	93.1938

same with the CS FGB. As the power lax index increases in z direction, the dimensionless axial stress $\bar{\sigma}_x$ decreases.

5.2.4. CF two-directional FGB

Finally, the results of elastostatic analysis of the CF FGB under uniformly distributed load are given in this example for various beam theories, gradation exponents and aspect ratios. As it is seen from Tables 13 and 14, the transverse deflections increase as the gradation exponent increases. Due to the higher stiffness, the dimensionless maximum transverse deflections values computed based on the EBT are smaller than the ones obtained by TBT and RBT for the aspect ratio set to 5. However, the computed results are very close to each other when the aspect ratio is set to 20.

In Fig. 9, the dimensionless transverse deflections of the CF FGB are plotted for various beam theories. The gradation exponent in z direction p_z is set to 1. The effect of the varying gradation exponent in x direction p_x is observed for the transverse deflections. As the gradation exponent in x direction increases, the deflections increase. Again, smaller deflections are obtained by using the EBT formulation.

It is observed that the dimensionless axial stress values computed by using EBT, TBT and RBT formulation are almost same, as shown in Fig. 10. The dimensionless shear stress values are shown in Fig. 11. As it is seen, the shear stress value obtained by the TBT is higher than the RBT. However, the computed shear stress values at the top and the bottom surface are zero, as expected based on the RBT formulation.

Table 14
Dimensionless maximum transverse deflections of the C-F FGB for different beam theories and gradation exponents, L/h = 20.

Theory	p_z	p_x				
		0	0.5	1	2	5
EBT	0	27.6324	28.9040	30.2570	33.1881	43.3767
	0.5	39.6381	41.2764	42.9833	46.5753	58.0487
	1	46.6597	48.4570	50.3113	54.1526	65.9210
	2	54.1156	56.0402	58.0056	62.0128	73.8132
	5	66.2063	68.2476	70.2990	74.3814	85.7472
TBT	0	27.7034	28.9853	30.3443	33.2894	43.5279
	0.5	39.7427	41.3876	43.1017	46.7100	58.2355
	1	46.7880	48.5927	50.4551	54.3137	66.1338
	2	54.2813	56.2140	58.1881	62.2130	74.0616
	5	66.4406	68.4900	70.5494	74.6473	86.0501
RBT	0	27.7394	29.0211	30.3809	33.3261	43.5644
	0.5	39.7882	41.4327	43.1474	46.7562	58.2821
	1	46.8487	48.6546	50.5149	54.3753	66.1949
	2	54.3809	56.3139	58.2881	62.3121	74.1563
	5	66.6396	68.6859	70.7424	74.8339	86.2201

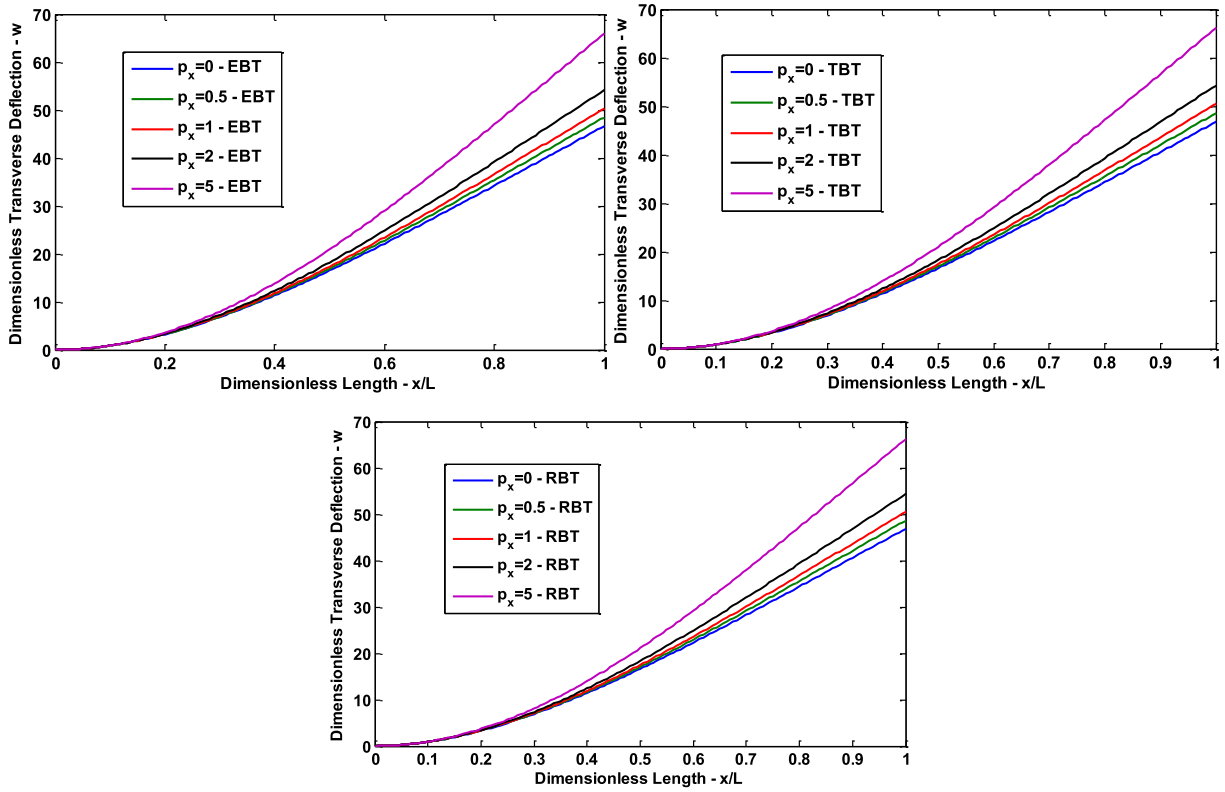

Fig. 9. Dimensionless transverse deflection values of the C-FFGB for different beam theories and gradation exponents in x direction, L/h = 20.

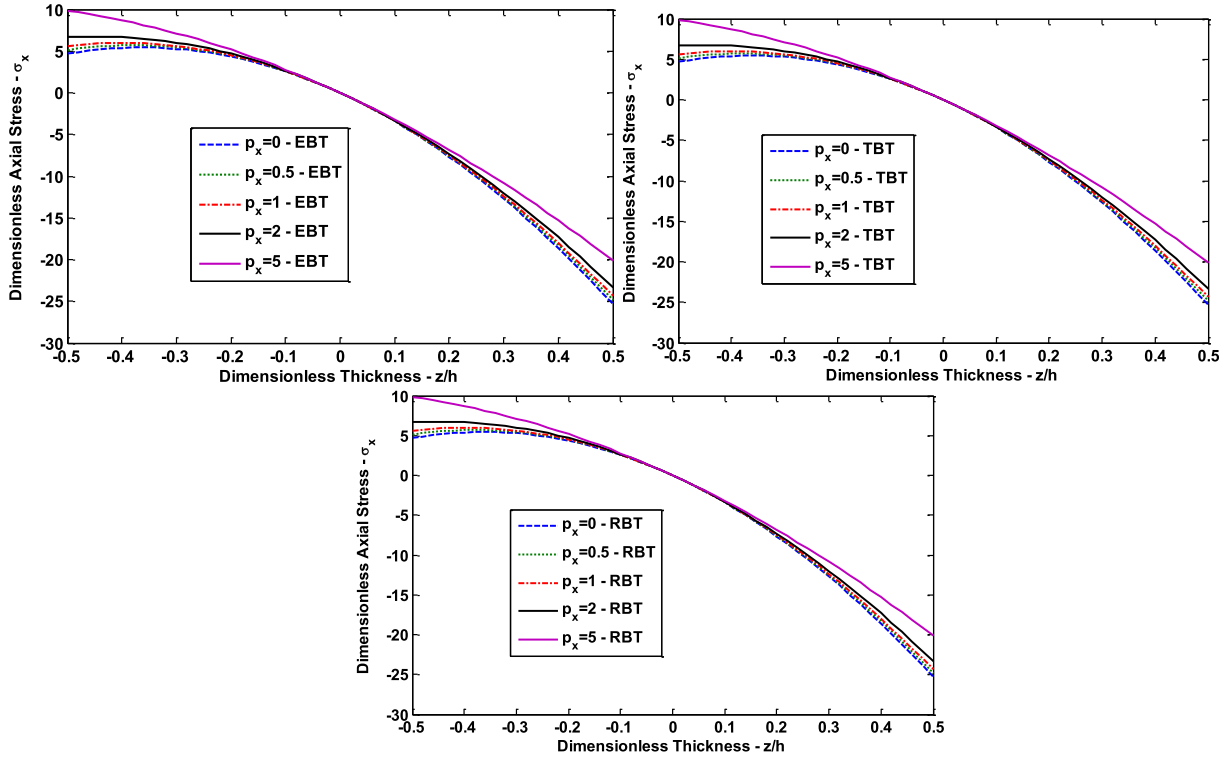

Fig. 10. Dimensionless axial stress $\bar{\sigma}_x\left(\frac{L}{2}, z\right)$ through the thickness of the C-F FGB for different beam theories and $p_z = 1$, L/h = 20.

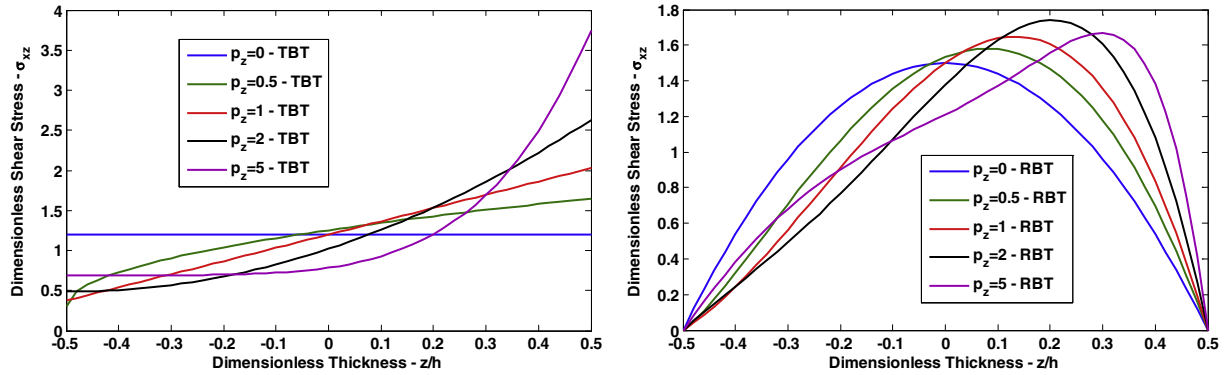

Fig. 11. Dimensionless transverse shear stress $\bar{\sigma}_{xz}(0, z)$ through the thickness of the C-F FGB for different beam theories and $p_x = 1$, L/h = 20.

6. Conclusion

The SSPH basis functions are employed to analyze the elastostatic behaviour of the two directional functionally graded beams subjected to different sets of boundary conditions and uniformly distributed load by using strong formulation of the problem. The EBT, TBT and RBT formulations are used to evaluate the transverse deflections, axial and shear stresses of two directional FGBs. The developed code is verified by using the results form previous studies and the analytical solutions. The numerical calculations are performed by using 161 nodes uniformly distributed in the problem domain and by employing 7 terms in the TSEs.

It is found that the SSPH method provides satisfactory expected results at least for the problems studied here. Based on the results of four numerical examples it is recommended that the SSPH method can be applied for solving linear two directional functionally graded beam problems by employing different shear deformation theories.

References

[1] Sankar BV. An elasticity solution for functionally graded beams. Compos Sci Technol 2001;61:689–96.
[2] Zhong Z, Yu T. Analytical solution of a cantilever functionally graded beam. Compos Sci Technol 2007;67:481–8.
[3] Nie GJ, Zhong Z, Chen S. Analytical solution for a functionally graded beam with arbitrary graded material properties. Composites Part B 2013;44:274–82.
[4] Ding HJ, Huang DJ, Chen WQ. Elasticity solutions for plane anisotropic functionally graded beams. Int J Solids Struct 2007;44:176–96.
[5] Kadoli R, Akhtar K, Ganesan N. Static analysis of functionally graded beams using higher order shear deformation theory. Appl Math Model 2008;32:2509–25.
[6] Li XF. A unified approach for analyzing static and dynamic behaviors of functionally graded Timoshenko and Euler-Bernoulli beams. J Sound Vib 2008;318:1210–29.
[7] Benatta MA, Mechab I, Tounsi A, Abbas ABE. Static analysis of functionally graded short beams including warping and shear deformation effects. Comput Mater Sci 2008;44:765–73.
[8] Ben-Oumrane S, Tounsi A, Mechab I, Mohamed BB, Mustapha M, Abbas ABE. Theoretical analysis of flexional bending of Al/Al_2O_3 S-FGM thick beams. Comput Mater Sci 2009;44:1344–50.

[9] Giunta G, Belouettar S, Carrera E. Analysis of FGM beams by means of classical and advanced theories. Mech Adv Mater Struct 2010;17:622–35.
[10] Menaa R, Tounsi A, Mouaici F, Mechab I, Zidi M, Bedia EAA. Analytical solutions for static shear correction factor of functionally graded rectangular beams. Mech Adv Mater Struct 2012;19:641–52.
[11] Li SR, Cao DF, Wan ZQ. Bending solutions of FGM Timoshenko beams from those of the homogenous Euler-Bernoulli beams. Appl Math Model 2013;37:7077–85.
[12] Vo TP, Thai HT, Nguyen TK, Inam F, Lee J. Static behaviour of functionally graded sandwich beams using a quasi-3D theory. Composites Part B 2015;68:59–74.
[13] Filippi M, Carrera E, Zenkour AM. Static analyses of FGM beams by various theories and finite elements. Composites Part B 2015;72:1–9.
[14] Jing LL, Ming PJ, Zhang WP, Fu LR, Cao YP. Static and free vibration analysis of functionally graded beams by combination Timoshenko theory and finite volume method. Compos Struct 2016;138:192–213.
[15] Aydogdu M, Taskin V. Free vibration analysis of functionally graded beams with simply supported edges. Mater Des 2007;28:1651–6.
[16] Sina SA, Navazi HM, Haddadpour H. An analytical method for free vibration analysis of functionally graded beams. Mater Des 2009;30:741–7.
[17] Simsek M. Fundamental frequency analysis of functionally graded beams by using different higher-order beam theories. Nucl Eng Des 2010;240:697–705.
[18] Simsek M, Kocaturk T. Free and forced vibration of a functionally graded beam subjected to a concentrated moving harmonic load. Compos Struct 2009;90:465–73.
[19] Simsek M. Vibration analysis of a functionally graded beam under a moving mass by using different beam theories. Compos Struct 2010;92:904–17.
[20] Sanjay AK, Gupta RK, Ramachandran P, Venkateswara RG. Free vibration analysis of functionally graded beams. Defence Sci J 2012;62(3):139–46.
[21] Mahi A, Adda Bedia EA, Tounsi A, Mechab I. An analytical method for temperature-dependent free vibration analysis of functionally graded beams with general boundary conditions. Compos Struct 2010;92:1877–87.
[22] Pradhan KK, Chakraverty S. Free vibration of Euler and Timoshenko functionally graded beams by Rayleigh-Ritz method. Composites Part B 2013;51:175–84.
[23] Pradhan KK, Chakraverty S. Effects of different shear deformation theories on free vibration of functionally graded beams. Int J Mech Sci 2014;82:149–60.
[24] Nuttawit W, Variddhi U. Free vibration analysis of functionally graded beams with general elastically end constraints by DTM. World J Mech 2012;2:297–310.
[25] Su H, Banerjee JR, Cheung CW. Dynamic stiffness formulation and free vibration analysis of functionally graded beams. Compos Struct 2013;106:854–62.
[26] Li SR, Wan ZG, Zhang JH. Free vibration of functionally graded beams based on both classical and first-order shear deformation beam theories. Appl Math Mech 2014;35:591–606.
[27] Aydogdu M. Thermal buckling analysis of cross-ply laminated composite beams with general boundary conditions. Compos Sci Technol 2007;67:1096–104.
[28] Kiani Y, Eslami MR. Thermal buckling analysis of functionally graded material beams. Int J Mech Mater Des 2010;6:229–38.
[29] Shahba A, Attarnejad R, Marvi MT, Hajilar S. Free vibration and stability analysis of axially functionally graded tapered Timoshenko beams with classical and non-classical boundary conditions. Composites Part B 2011;42:801–8.
[30] Nateghi A, Salamat-talab M, Rezapour J, Daneshian B. Size dependent buckling analysis of functionally graded micro beams based on modified couple stress theory. Appl Math Model 2012;36:4971–87.
[31] Akgöz B, Civalek Ö. Buckling analysis of functionally graded microbeams based on the strain gradient theory. Acta Mech 2013;224:2185–201.
[32] Nemat-Alla M. Reduction of thermal stresses by developing two-dimensional functionally graded materials. Int J Solids Struct 2003;40:7339–56.
[33] Goupee AJ, Vel SS. Optimization of natural frequencies of bidirectional functionally graded beams. Struct Multidisc Optim 2006;32:473–84.
[34] Lü CF, Chen WQ, Xu RQ, Lim CW. Semi-analytical elasticity solutions for bidirectional functionally graded beams. Int J Solids Struct 2008;45:258–75.
[35] Aydogdu M. Semi-inverse method for vibration and buckling of axially functionally graded beams. J Reinf Plast Compos 2008;27:683–91.
[36] Huang Y, Li XF. Buckling analysis of nonuniform and axially graded columns with varying flexural rigidity. J Eng Mech 2011;137(1):73–81.
[37] Zhao L, Chen WQ, Lü CF. Symplectic elasticity for two-directional functionally graded materials. Mech Mater 2012;54:32–42.
[38] Simsek M. Buckling of Timoshenko beams composed of two-dimensional functionally graded material (2D-FGM) having different boundary conditions. Compos Struct 2016;149:304–14.
[39] Donning BM, Liu WK. Meshless methods for shear-deformable beams and plates. Comput Methods Appl Mech Eng 1998;152:47–71.
[40] Gu YT, Liu GR. A local point interpolation method for static and dynamic analysis of thin beams. Comput Methods Appl Mech Eng 2001;190 (42):5515–28.
[41] Ferreira AJM, Roque CMC, Martins PALS. Radial basis functions and higher-order shear deformation theories in the analysis of laminated composite beams and plates. Compos Struct 2004;66:287–93.
[42] Ferreira AJM, Fasshauer GE. Computation of natural frequencies of shear deformable beams and plates by an RBF-pseudospectral method. Comput Methods Appl Mech Eng 2006;196:134–46.
[43] Moosavi MR, Delfanian F, Khelil A. The orthogonal meshless finite volume method for solving Euler-Bernoulli beam and thin plate problems. Thin-Walled Structures 2011;49:923–32.
[44] Wu CP, Yang SW, Wang YM, Hu HT. A meshless collocation method for the plane problems of functionally graded material beams and plates using the DRK interpolation. Mech Res Commun 2011;38:471–6.
[45] Roque CMC, Figaldo DS, Ferreira AJM, Reddy JN. A study of a microstructure-dependent composite laminated Timoshenko beam using a modified couple stress theory and a meshless method. Compos Struct 2013;96:532–7.
[46] Lucy LB. A numerical approach to the testing of the fission hypothesis. Astron J 1977;82:1013–24.
[47] Chen JK, Beraun JE, Jin CJ. An improvement for tensile instability in smoothed particle hydrodynamics. Comput Mech 1999;23:279–87.
[48] Chen JK, Beraun JE, Jin CJ. Completeness of corrective smoothed particlemethod for linear elastodynamics. Comput Mech 1999;24:273–85.
[49] Liu WK, Jun S, Zhang YF. Reproducing kernel particle methods. Int J Numer Meth Fluids 1995;20:1081–106.
[50] Liu WK, Jun S, Li S, Adee J, Belytschko T. Reproducing kernel particle methods for structural dynamics. Int J Numer Meth Eng 1995;38:1655–79.
[51] Chen JS, Pan C, Wu CT, Liu WK. Reproducing kernel particlemethods for large deformation analysis of non-linear structures. Comput Methods Appl Mech Eng 1996;139:195–227.
[52] Zhang GM, Batra RC. Modified smoothed particle hydrodynamics method and its application to transient problems. Comput Mech 2004;34:137–46.
[53] Batra RC, Zhang GM. Analysis of adiabatic shear bands in elasto-thermo-viscoplastic materials by modified smoothed particle hydrodynamics (MSPH) method. J Comput Phys 2004;201:172–90.
[54] Zhang GM, Batra RC. Wave propagation in functionally graded materials by modified smoothed particle hydrodynamics (MSPH) method. J Comput Phys 2007;222:374–90.
[55] Batra RC, Zhang GM. Search algorithm, and simulation of elastodynamic crack propagation by modified smoothed particle hydrodynamics (MSPH) method. Comput Mech 2007;40:531–46.
[56] Zhang GM, Batra RC. Symmetric smoothed particle hydrodynamics (SSPH) method and its application to elastic problems. Comput Mech 2009;43:321–40.
[57] Batra RC, Zhang GM. SSPH basis functions for meshless methods, and comparison of solutions with strong and weak formulations. Comp Mech 2008;41:527–45.
[58] Tsai CL, Guan YL, Batra RC, Ohanehi DC, Dillard JG, Nicoli E, Dillard DA. Comparison of the performance of SSPH and MLS basis functions for two-dimensional linear elastostatics problems including quasistatic crack propagation. Comput Mech 2013;51:19–34.
[59] Tsai CL, Guan YL, Ohanehi DC, Dillard JG, Dillard DA, Batra RC. Analysis of cohesive failure in adhesively bonded joints with the SSPH meshless method. Int J Adhes Adhes 2014;51:67–80.
[60] Karamanli A, Mugan A. Solutions of two-dimensional heat transfer problems by using symmetric smoothed particle hydrodynamics method. J Appl Comp Math 2012;1:1–6.
[61] Karamanli A. Bending deflection analysis of a semi-trailer chassis by using symmetric smoothed particle hydrodynamics. Int J Eng Technol 2015;1 (4):134–40.
[62] Karamanli A, Mugan A. Strong from meshless implementation of Taylor series method. Appl Math Comput 2013;219:9069–80.
[63] Karamanli A. Different implementation approaches of the strong form meshless implementation of Taylor series method. Int J Eng Technol 2015;1 (3):95–105.
[64] Kaewumpai S, Luadsong A. Two-field-variable meshless method based on moving kriging interpolation for solving simply supported thin plates under various loads. J King Saud Univ Sci 2014:1018–3647.
[65] Yimnak K, Luadsong A. A local integral equation formulation based on moving kriging interpolation for solving coupled nonlinear reaction–diffusion equations. Advances in Mathematical Physics 2014.
[66] Zhuang X, Zhu H, Augarde C. The meshless Shepard and least squares (MSLS) method. Comput Mech 2014;53:343–57.
[67] Fatahi H, Nadjafi JS, Shivanian E. New spectral meshless radial point interpolation (SMRPI) method for the two-dimensional Fredholm integral equations on general domains with error analysis. J Comput Appl Math 2016;264:196–209.
[68] Love AEH. A treatise on the mathematical theory of elasticity. 4th ed. New York: Dover Publications; 1927.
[69] Timoshenko SP, Goodier JC. Theory of elasticity. New York: McGraw-Hill Co., Inc.; 1970.
[70] Wang CM, Reddy JN, Lee KH. Shear deformable beams and plates relations with classical solutions. Oxford: Elsevier Science Ltd.; 2000.
[71] Polizzotto C. From the Euler-Bernoulli beam to the Timoshenko one through a sequence of Reddy-type shear deformable beam models of increasing order. Eur J Mech A/Solids 2015;53:62–74.
[72] Levinson M. A new rectangular beam theory. J Sound Vib 1981;74: 81–7.
[73] Bickford WB. A consistent higher order beam theory. Dev Theor Appl Mechan 1982;11:137–50.
[74] Heyliger PR, Reddy JN. A higher order beam finite element for bending and vibration problems. J Sound Vib 1988;126(2):309–26.
[75] Subramanian P. Dynamic analysis of laminated composite beams using higher order theories and finite elements. Compos Struct 2006;73:342–53.

[76] Reddy JN. Nonlocal theories for bending, buckling and vibration of beams. Int J Eng Sci 2007;45:288–307.
[77] Carrera E, Giunta G. Refined beam theories based on a unified formulation. Int J Appl Mech 2010;2(1):117–43.
[78] Giunta G, Biscani F, Bellouettar S, Ferreira AJM, Carrera E. Free vibration analysis of composite beams via refined theories. Composites Part B 2013;44:540–52.
[79] Arya H. A new zig-zag model for laminated composite beams: free vibration analysis. J Sound Vib 2003;264:485–90.
[80] Jun L, Hongxing H. Dynamic stiffness analysis of laminated composite beams using trigonometric shear deformation theory. Compos Struct 2009;89:433–42.
[81] Kurama M, Afaq KS, Mistou S. Mechanical behavior of laminated composite beams by the new multi-layered laminated composite structures model with trigonometric shear stress continuity. Int J Solids Struct 2003;40:1525–46.
[82] Li XF, Wang BL, Han JC. A higher-order theory for static and dynamic analyses of functionally graded beams. Arch Appl Mech 2010;80:1197–212.